Accurate High-Maneuvering Trajectory Tracking for Quadrotors: A Drag Utilization Method

Jindou Jia, Kexin Guo, Xiang Yu, Weihua Zhao, and Lei Guo*

***Abstract*— The balanceness between the tracking performance and the aerodynamic drag treatment is of paramount importance especially in the presence of the quadrotor aggressive maneuvers. Different from standard approaches that achieve precise tracking by feedforward compensating the estimated drag, this work presents a scheme to appropriately utilize drag. By means of the proposed drag-utilization scheme, the disturbance absorption can be achieved. In addition to eliminate the adverse effect, the control gains are subtly enlarged with less noise. Moreover, an adaptive law for estimating the drag coefficients onboard is provided. Subsequently, the wind disturbance is explicitly considered at the control design stage. A wind speed observer (WSO) is designed to improve the tracking performance, based on current velocity and attitude. Compared with the traditional disturbance observer (DO), the proposed WSO can not only fully utilize the disturbance characteristic but also contribute to reduce the control conservativeness. In experiments, two types of quadrotors with different thrust-to-weight ratios (TWRs) are employed to evaluate the applicability of the presented scheme. Comparative results show that the proposed scheme outperforms several popular methods.**

I. Introduction

Quadrotor unmanned aerial vehicles (UAVs) with high agility have received increasing interest in many scenarios, such as search-and-rescue, entertainment, and logistics [1]–[4]. In an attempt to achieve high maneuverability, various advanced methods have been proposed in last decades, including differential flatness-based control (DFBC) [5], [6] and model predictive control (MPC) [7], [8], just to mention a few. However, when suffering from external disturbances, how to achieve accurate tracking in an agile flight is still challenging [9]–[11].

Manuscript received: November, 21, 2021; Revised: February, 20, 2022; Accepted: April, 19, 2022.

This paper was recommended for publication by Editor Pauline Pounds upon evaluation of the Associate Editor and Reviewers' comments.

This work was supported in part by the National Key Research and Development Program of China (Grant No. 2020YFA0711200), National Natural Science Foundation of China (Grant No. 61833013, 61973012, and 61903019), Defense Industrial Technology Development Program (Grant No. JCKY2020601C016), Key Research and Development Program of Zhejiang (Grant No. 2021C03158), Science and Technology Key Innovative Project of Hangzhou (Grant No. 20182014B06), Natural Science Foundation of Zhejiang Province (Grant No. LD21F030001 and LQ20F030006), and Outstanding Research Project of Shen Yuan Honors College, BUAA (Grant No. 230121101).

J. Jia, X. Yu, and L. Guo are with the School of Automation Science and Electrical Engineering, Beihang University, 100191, Beijing, China. E-mail: {jdjia, xiangyu_buaa, lguo}@buaa.edu.cn.

J. Jia is also with Shenyuan Honors College, Beihang University, 100191, Beijing, China.

K. Guo is with the School of Aeronautic Science and Engineering, Beihang University, 100191, Beijing, China. E-mail: kxguo@buaa.edu.cn.

W. Zhao is with the Tyiee Technology Company, 518110, Shenzhen, China. E-mail: zhao0079@e.ntu.edu.sg.

* Corresponding author.

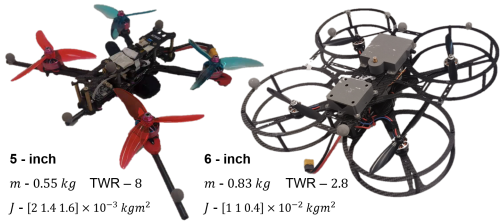

Fig. 1. Quadrotors used in the experiments. Flight video can be found at https://youtu.be/qO8A6lwCxMU.

Aerodynamic drag is the dominant disturbance as the quadrotor maneuvers aggressively [6]. The sources of aerodynamic drag mainly consist of the parasite drag and induced drag. Plenty of works have been devoted to represent the aerodynamic drag mathematically [12]–[16]. In [12], [13], the aerodynamic drag is represented as a function of the relative airspeed ($\boldsymbol{v}_a = \boldsymbol{v} - \boldsymbol{v}_w$, where $\boldsymbol{v}_a \in \mathbb{R}^3$, $\boldsymbol{v} \in \mathbb{R}^3$, and $\boldsymbol{v}_w \in \mathbb{R}^3$ denote the relative airspeed, quadrotor speed, and wind speed in internal frame, respectively). The impact of attitude change is additionally considered in [14]–[16]. Especially, in [14], a simplified and effective representation is constructed ($-\boldsymbol{R}\boldsymbol{D}\boldsymbol{R}^T\boldsymbol{v}_a$, where $\boldsymbol{D} \in \mathbb{R}^{3\times3}$ represents drag coefficients and $\boldsymbol{R} \in \mathbb{R}^{3\times3}$ denotes rotation matrix from body frame to inertial frame). In order to eliminate the adverse impact caused by aerodynamic drag, a common practice is to adopt a feedforward compensation scheme [4], [6]. Under such compensation scheme, the drag coefficients are usually obtained by parameter identification techniques and the aerodynamic drag is thereby compensated.

Apart from the aerodynamic drag, another factor that limits the performance is the controller gain. Within the control capability of configured actuators, the tracking performance usually tends to be better as the controller gains increase proportionally. However, due to sensor noise, delays, finite control frequency, and actuator limitation, the gains cannot be infinite. For example, in the presence of the noise in the processed velocity, the "high-frequency vibration" phenomenon will be exacerbated as the relative gains increase abruptly.

In this paper, a drag-utilization scheme is presented to handle the aerodynamic drag and enlarge the controller gain meanwhile. It is well known that the aerodynamic drag largely depends on the quadrotor speed in the absence of wind ($\boldsymbol{v}_w = 0$), which implies that the aerodynamic drag might induce damping effect as the derivative portion does within a PID control scheme. Especially, such a natural drag

has no calculated noise in essence. It's an interesting question that is it possible to utilize the natural aerodynamic drag appropriately? In this paper, distinguishing from the precious direct compensation method [4], [6], a drag-utilization scheme inspired by [17], [18] is exploited for the sake of high maneuvering flight. By treating the aerodynamic drag as a damping term and adding the corresponding expected signal, the additional control gain can be generated with less noise as compared to the compensation scheme.

Next, as $\boldsymbol{v}_w \neq 0$, the aerodynamic drag caused by wind ($\boldsymbol{RDR}^T\boldsymbol{v}_w$) needs to be handled. Since a reliable and lightweight wind sensor for micro quadrotors is not available [12], [19], it is extremely difficult to measure external wind velocity onboard. In consequence, the drag feedforward compensation scheme relying on the relative wind speed cannot be applied. For handing wind disturbances, disturbance observer (DO) is usually designed [20]–[22], where the wind disturbance ($\boldsymbol{RDR}^T\boldsymbol{v}_w$) is assumed to be bounded or derivative bounded. The bound usually determines the steady-state tracking errors [23]. The DO-based control scheme is somehow conservative without fully utilizing the characteristics of aerodynamic drag. In this paper, a novel wind speed observer (WSO) is proposed to directly estimate the external wind speed $\boldsymbol{v}_w$ instead of $\boldsymbol{RDR}^T\boldsymbol{v}_w$, reducing the conservativeness of control.

The outline of the paper is as follows. Section II reviews related previous works briefly. Section III provides the required notations and quadrotor dynamics that will be employed in the latter parts. Section IV goes into details on the control scheme. Section V presents the experimental results from the real world flights. Section VI discusses the limitations of the proposed methods. Finally, Section VII concludes this article.

II. Related Work

A. Aggressive Control

In recent years, aggressive control methods for the quadrotor have achieved significant progress. DFBC [5] has been prosperous due to the features of less computation and easy implementation. To circumvent singularities [24] in the differential flatness transformation, the Hopf Fibration on $SO(3)$ is used to hit almost all singularities in [25]. In recent years, thanks to developments in hardware and algorithmic efficiency, MPC methods have been applied in quadrotor [7], [8], which can handle constraints efficiently. However, MPC methods suffer from numerical convergence issues and rely on accurete dynamic representation [8].

When either system uncertainty or external disturbance is involved, the incremental nonlinear dynamic inversion (INDI) method is proposed in [8] and [26] to improve the anti-disturbance ability. In [27], neural network (NN) is employed to establish an identity mapping function from the desired output to the actual output between the planning module and the control module. In [9], the disturbances on translational and rotational loops arising from wind are compensated by an artificial NN whose weights are adjusted online. However, the above anti-disturbance methods treat the uncertainty and external disturbance as a lumped disturbance without further utilizing the disturbance information.

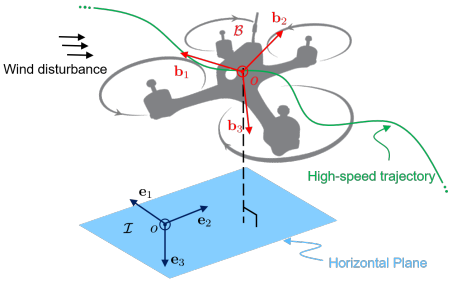

Fig. 2. Schematic of a quadrotor.

B. Aerodynamic Drag Rejection

To overcome the aerodynamic drag in high-speed flights, efficient drag modeling approaches are investigated [13], [14], [28]. The first-order aerodynamic drag model is established in [14] and proven to be differentially flat in [6]. In [6], a gradient-free optimization approach is adopted to identify drag coefficients offline and the drag is compensated in a cascaded control law intuitively. The similar feedforword compensation scheme is also applied in other works [4], [29].

When encountering wind disturbances, DO is usually designed to estimate the adverse effect. In [20], a frequency domain DO is designed to estimate the wind disturbance. Whereas, only the linearized model is considered, which cannot cover the entire operation state of the quadrotor. Focusing on this system with multi-disturbances, composite hierarchical anti-disturbance control (CHADC) design is firstly proposed in [30], which properly handles the limitations of disturbance homogeneousness, internal stability, and disturbance invariance in traditional anti-disturbance control scheme. Within the framework of CHADC, the extended state observers (ESOs) are exploited to estimate the wind disturbance with derivative-bounded assumption [22]. In [31], the extended Kalman filter is employed to estimate the wind disturbance based on the feedback of ESC motor commands. The aforementioned studies [20], [22], [31] regard the wind effect as a lumped disturbance, without further exploring its inherent characteristic (the relationship with attitude). The rough assumptions on wind effect (bound or derivative-bounded) also affect the stability proof procedure.

In [32], a novel coupled nonlinear velocity aided attitude filter is proposed to estimate quadrotor states and external wind speed. Although efficient experiment results are shown, the stability proof is not provided when the wind estimation is considered. Different from [32], to improve the tracking performance, a more portable WSO is designed based on velocity and attitude measurements, whilst the stability can be guaranteed.

III. Preliminaries

A. Notations

Throughout this paper, $\mathbb{R}$ denotes the set of real numbers, the operator $\|\cdot\|$ represents the standard Euclidean norm for

vectors or the corresponding induced norm for matrices, the operator $\circ$ is the quaternion multiplication, $\lambda(\cdot)$, $\lambda_M(\cdot)$, and $\lambda_m(\cdot)$ represent the eigenvalue, maximum eigenvalue, and minimum eigenvalue of a matrix, $tr(\cdot)$ represents the trace of a matrix, and $(\cdot)_d$ denotes the corresponding desired signal. As a convention, the skew-symmetric operator of a vector $\boldsymbol{x} = \begin{bmatrix} x_1 & x_2 & x_3 \end{bmatrix}^\top \in \mathbb{R}^3$ is defined as

$$\boldsymbol{x}^\times = \begin{bmatrix} 0 & -x_3 & x_2 \\ x_3 & 0 & -x_1 \\ -x_2 & x_1 & 0 \end{bmatrix} \in \mathbb{R}^{3\times 3}.$$

In reverse, the vee-map $(\cdot)^\vee$ is defined as the inverse of the cross-map: $(\boldsymbol{x}^\times)^\vee = \boldsymbol{x}$.

As depicted in Fig. 2, two frames are defined to describe the state of the quadrotor: inertial frame $\mathcal{I} = [\boldsymbol{e}_1, \boldsymbol{e}_2, \boldsymbol{e}_3]$ and body frame $\mathcal{B} = [\boldsymbol{b}_1, \boldsymbol{b}_2, \boldsymbol{b}_3]$. Moreover, m is the mass of the quadrotor, g is the gravitational acceleration, $\boldsymbol{J} \in \mathbb{R}^{3\times 3}$ is the inertia matrix in $\mathcal{B}$, $\boldsymbol{p} \in \mathbb{R}^3$, $\boldsymbol{v} \in \mathbb{R}^3$, and $\boldsymbol{a} \in \mathbb{R}^3$ represents the position, velocity, and acceleration in $\mathcal{I}$ respectively, $\boldsymbol{q} \in \mathbb{R}^4$ is the relative orientation between $\mathcal{I}$ and $\mathcal{B}$, $\boldsymbol{\omega} \in \mathbb{R}^3$ and $\boldsymbol{\alpha} \in \mathbb{R}^3$ are the angular velocity and angular acceleration in $\mathcal{B}$, and $\boldsymbol{R} \in \mathbb{R}^{3\times 3}$ represents the rotation matrix from $\mathcal{B}$ to $\mathcal{I}$. For the system control inputs, $f \in \mathbb{R}$ is the the total thrust magnitude along $\boldsymbol{b}_3$ and $\boldsymbol{\tau} \in \mathbb{R}^3$ is the control moment input of the rotational loop in $\mathcal{B}$.

B. Quadrotor Model

The kinematics and dynamics of the quadrotor can be modeled as follows,

$$\begin{cases} \dot{\boldsymbol{p}} = \boldsymbol{v}, \\ \dot{\boldsymbol{R}} = \boldsymbol{R}\boldsymbol{\omega}^\times, \end{cases} \tag{1}$$

$$\begin{cases} m\boldsymbol{a} = -f\boldsymbol{b}_3 + mg\boldsymbol{e}_3 + \boldsymbol{F}_w, \\ \boldsymbol{J}\dot{\boldsymbol{\omega}} = -\boldsymbol{\omega}^\times \boldsymbol{J}\boldsymbol{\omega} + \boldsymbol{\tau}, \end{cases} \tag{2}$$

where $\boldsymbol{F}_w \in \mathbb{R}^3$ represents the aerodynamic drag, and its first-order form is employed in the paper,

$$\begin{aligned} \boldsymbol{F}_w &= -\boldsymbol{R}\boldsymbol{D}\boldsymbol{R}^T\boldsymbol{v}_a, \\ &= \underbrace{-\boldsymbol{R}\boldsymbol{D}\boldsymbol{R}^T\boldsymbol{v}}_{\boldsymbol{F}_{w1}} + \underbrace{\boldsymbol{R}\boldsymbol{D}\boldsymbol{R}^T\boldsymbol{v}_w}_{\boldsymbol{F}_{w2}}, \end{aligned} \tag{3}$$

where $\boldsymbol{D} = diag(d_{11}, d_{22}, d_{33}) \in \mathbb{R}^{3\times 3}$ is a constant diagonal matrix formed by the mass-normalized drag coefficients. Refer to [14] for more details. Other drag effects in [14] are neglected in this paper, which have minor effects on the tracking performance [6]. From (3), it is obvious that the aerodynamic drag depends not only on the velocity $\boldsymbol{v}_a$, but also on the attitude $\boldsymbol{R}\boldsymbol{D}\boldsymbol{R}^T$. In this work, the two parts $\boldsymbol{F}_{w1}$ and $\boldsymbol{F}_{w2}$ in (3) are handled by using the divide and conquer method.

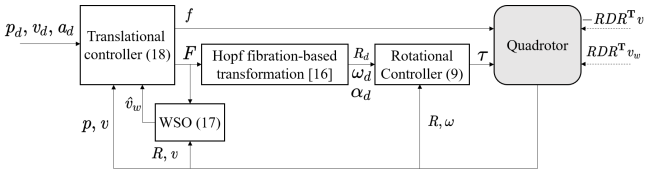

Fig. 3. The control diagram of the designed cascade controller.

IV. Methods

In this section, the main control scheme is presented, as shown in Fig. 3. Firstly, the baseline controller is designed without considering the aerodynamic drag. Secondly, the drag-utilization scheme is presented to handle $\boldsymbol{F}_{w1}$ and an adaptive law for estimating the drag coefficients online is provided. Finally, a WSO is designed to estimate the wind speed $\boldsymbol{v}_w$, which is fed into baseline controller to reject $\boldsymbol{F}_{w2}$. Each step is accompanied by a stability analysis.

A. Baseline Controller

Similar to [22], suppose that bandwidth of the rotational control loop is significantly higher than the bandwidth of the translational control loop. Then, the translational controller may be designed to be largely independent of the dynamics of the rotational control loop.

Define the position tracking error $\boldsymbol{e}_p = \boldsymbol{p}_d - \boldsymbol{p} \in \mathbb{R}^3$, where $\boldsymbol{p}_d \in \mathbb{R}^3$ is the desired position from the planning module. Hence, the reference velocity $\boldsymbol{v}_r \in \mathbb{R}^3$ and acceleration $\boldsymbol{a}_r \in \mathbb{R}^3$ are designed as

$$\boldsymbol{v}_r = \boldsymbol{v}_d + \boldsymbol{K}_P\boldsymbol{e}_p, \tag{4}$$

$$\boldsymbol{a}_r = \dot{\boldsymbol{v}}_r, \tag{5}$$

where $\boldsymbol{v}_d \in \mathbb{R}^3$ is the desired velocity and $\boldsymbol{K}_P \in \mathbb{R}^{3\times 3}$ is a positive diagonal gain matrix. $\boldsymbol{v}_r$ can be interpreted as the modified desired velocity by considering position tracking error. Subsequently, define a sliding variable $\boldsymbol{s} = \boldsymbol{v}_r - \boldsymbol{v}$. The control objective is to design a feedback controller to achieve $\boldsymbol{s} \to 0$, such that $\boldsymbol{e}_p$ can converge to zero exponentially.

In the absence of the aerodynamic drag, the translational baseline controller is designed as

$$\boldsymbol{F}_0 = -mg\boldsymbol{e}_3 + m\boldsymbol{a}_r + \boldsymbol{K}_D\boldsymbol{s}, \tag{6}$$

where $\boldsymbol{K}_D \in \mathbb{R}^{3\times 3}$ is a positive diagonal gain matrix.

Construct the Lyapunov function as:

$$V_1 = \frac{m}{2}\boldsymbol{s}^T\boldsymbol{s}. \tag{7}$$

By letting $-f\boldsymbol{b}_3 = \boldsymbol{F}_0$, differentiating (7) gives

$$\begin{aligned} \dot{V}_1 &\overset{(a)}{=} \boldsymbol{s}^T\left(m\boldsymbol{a}_r - (-f\boldsymbol{b}_3 + mg\boldsymbol{e}_3 + \boldsymbol{F}_w)\right) \\ &\overset{(b)}{=} -\boldsymbol{s}^T\boldsymbol{K}_D\boldsymbol{s} - \boldsymbol{s}^T\boldsymbol{F}_w, \end{aligned} \tag{8}$$

where (a) is followed from (2) and (5) and (b) is followed from (6). It can be seen from (8), if the aerodynamic drag $\boldsymbol{F}_w$ is neglected, one can render

$$\dot{V}_1 \leq -\frac{2\lambda_m(\boldsymbol{K}_D)}{m}V_1. \tag{9}$$

which leads to $V_1(t) \leq V_1(0) e^{-c_1 t}$, where $c_1 = \frac{2\lambda_m(\boldsymbol{K}_D)}{m}$. It is obvious that $\boldsymbol{s} \to 0$ exponentially as $t \to \infty$.

By virtue of a differential flatness scheme, the desired attitude $\boldsymbol{R}_d \in \mathbb{R}^{3\times3}$, attitude velocity $\boldsymbol{\omega}_d \in \mathbb{R}^3$, and attitude acceleration $\boldsymbol{\alpha}_d \in \mathbb{R}^3$ can be obtained from the output of position loop and the higher order derivatives of desired position [5]. To avoid the singularities, the Hopf fibration based-transformation is employed in this work. The transformal procedure is omitted herein for the sake of simplicity. More details can be found in [25].

The rotational geometric control scheme is employed,

$$\begin{aligned}\boldsymbol{\tau}_0 = &\boldsymbol{K}_R \frac{1}{2}\left(\boldsymbol{R}^T\boldsymbol{R}_d - \boldsymbol{R}_d^T\boldsymbol{R}\right)^\vee + \boldsymbol{K}_\omega(\boldsymbol{\omega}_d - \boldsymbol{\omega}) + \boldsymbol{\omega}\times\boldsymbol{J}\boldsymbol{\omega} \\ &-\boldsymbol{J}\left(\boldsymbol{\omega}^\times\boldsymbol{R}^\top\boldsymbol{R}_d\boldsymbol{\omega}_d - \boldsymbol{R}^\top\boldsymbol{R}_d\boldsymbol{\alpha}_d\right),\end{aligned} \tag{10}$$

where $\boldsymbol{K}_R \in \mathbb{R}^{3\times3}$ and $\boldsymbol{K}_\omega \in \mathbb{R}^{3\times3}$ are the diagonal gain matrices. By resorting to this geometric controller, the rotational loop is exponentially stable if the initial conditions satisfy $\Psi(\boldsymbol{R}(0), \boldsymbol{R}_d(0)) < 2$ and $\|\boldsymbol{\omega}_d(0) - \boldsymbol{\omega}(0)\|^2 < \frac{2}{\lambda_M(\boldsymbol{J})}\boldsymbol{K}_R(2 - \Psi(\boldsymbol{R}(0), \boldsymbol{R}_d(0)))$, where $\Psi(\boldsymbol{R}, \boldsymbol{R}_d) = \frac{1}{2}tr\left[\boldsymbol{I} - \boldsymbol{R}_d^T\boldsymbol{R}\right]$. Please refer to [33] for more proof details.

Till now, the baseline controller is formalized and the stability of the quadrotor system can be guaranteed without considering the aerodynamic drag. In the next subsection, a drag-utilization scheme is developed to handle the aerodynamic drag and improve $\boldsymbol{K}_D$ limitation problem.

B. Drag-utilization Scheme

As long as the aerodynamic drag ($-\boldsymbol{R}\boldsymbol{D}\boldsymbol{R}^T\boldsymbol{v}$) is treated as a damping term, a modified translational loop can be constructed as

$$\boldsymbol{F}_1 = -mg\boldsymbol{e}_3 + m\boldsymbol{a}_r + \boldsymbol{K}_D\boldsymbol{s} + \boldsymbol{R}\boldsymbol{D}\boldsymbol{R}^T\boldsymbol{v}_r, \tag{11}$$

where $\boldsymbol{D}$ can be obtained by fitting priori experimental data, just like in [6]. In this paper (Section IV-B.1), an online adaptive estimation method is also provided to achieve an approximation of $\boldsymbol{D}$.

By employing the controller (11) and assuming the external wind speed $\boldsymbol{v}_w = 0$ ($\boldsymbol{v}_w \neq 0$ is handled later in Section IV-C), (8) can be adjusted as

$$\dot{V}_1' = -\boldsymbol{s}^T\left(\boldsymbol{K}_D + \boldsymbol{R}\boldsymbol{D}\boldsymbol{R}^T\right)\boldsymbol{s}, \tag{12}$$

where V_1' denotes the same Lyapunov function structure as (7), under controller (11). Due to $\boldsymbol{R}\boldsymbol{D}\boldsymbol{R}^T$ and $\boldsymbol{D}$ are similar matrices, their eigenvalues are the same and positive. Then, it can be proven that

$$\dot{V}_1' \leq -\frac{2\left(\lambda_m(\boldsymbol{K}_D) + \lambda_m(\boldsymbol{D})\right)}{m}V_1', \tag{13}$$

which leads to $V_1'(t) \leq V_1'(0) e^{-c_2 t}$, where $c_2 = \frac{2(\lambda_m(\boldsymbol{K}_D)+\lambda_m(\boldsymbol{D}))}{m}$.

Remark 1. *Compared with the compensation scheme [4], the drag utilization scheme adopts to add a reference term $\boldsymbol{R}\boldsymbol{D}\boldsymbol{R}^T\boldsymbol{v}_r$ instead of a compensated term $\boldsymbol{R}\boldsymbol{D}\boldsymbol{R}^T\boldsymbol{v}$, which does not induce calculated noise from $\boldsymbol{v}$. Notice that added $\boldsymbol{R}\boldsymbol{D}\boldsymbol{R}^T\boldsymbol{v}_r$ induces the noise from $\boldsymbol{p}$. Nevertheless, the noise in $\boldsymbol{p}$ is usually slighter than that in $\boldsymbol{v}$. What is more, by comparing (13) with (9), it can be obtained that the convergence speed of the tracking error $\boldsymbol{s}$ is improved, which cannot be achieved by the existing schemes.*

From another point of view, the drag-utilization scheme can enlarge the control gain $\boldsymbol{K}_D$. The drag utilization scheme adopts to add a reference term $\boldsymbol{R}\boldsymbol{D}\boldsymbol{R}^T\boldsymbol{v}_r$, which can combine with the suffered drag $-\boldsymbol{R}\boldsymbol{D}\boldsymbol{R}^T\boldsymbol{v}$ to obtain $\boldsymbol{R}\boldsymbol{D}\boldsymbol{R}^T\boldsymbol{s}$. Then the control gain of $\boldsymbol{s}$ becomes $\boldsymbol{R}\boldsymbol{D}\boldsymbol{R}^T + \boldsymbol{K}_D$.

1) Drag Coefficient Estimation: An adaptive law is provided to obtain an approximation of $\boldsymbol{D}$ in addition, which will be used for comparison in Section V.

By letting $\boldsymbol{d} = \begin{bmatrix} d_{11} & d_{22} & d_{33} \end{bmatrix}^T \in \mathbb{R}^3$ that represents the constrictive form of $\boldsymbol{D}$, $\begin{bmatrix} q_1 & q_2 & q_3 \end{bmatrix}^T = \boldsymbol{R}^T\boldsymbol{v}_r$, and $\boldsymbol{Q} = diag(q_1, q_2, q_3) \in \mathbb{R}^{3\times3}$, it can be proven that

$$\boldsymbol{R}\boldsymbol{D}\boldsymbol{R}^T\boldsymbol{v}_r = \boldsymbol{R}\boldsymbol{Q}\boldsymbol{d}. \tag{14}$$

Denote the estimated drag coefficient as $\hat{\boldsymbol{d}} \in \mathbb{R}^3$. Construct the Lyapunov candidate as

$$V_2 = \frac{m}{2}\boldsymbol{s}^T\boldsymbol{s} + \frac{1}{2}\tilde{\boldsymbol{d}}\boldsymbol{\Gamma}^{-1}\tilde{\boldsymbol{d}}, \tag{15}$$

where $\tilde{\boldsymbol{d}} = \boldsymbol{d} - \hat{\boldsymbol{d}} \in \mathbb{R}^3$ is the estimation errors of the drag coefficient and $\boldsymbol{\Gamma} \in \mathbb{R}^{3\times3}$ is a positive diagonal matrix.

Similar to the derivation procedure of (8), differentiating (15) renders

$$\dot{V}_2 = -\boldsymbol{s}^T\left(\boldsymbol{K}_D + \boldsymbol{R}\boldsymbol{D}\boldsymbol{R}^T\right)\boldsymbol{s} + \boldsymbol{s}^T\boldsymbol{R}\boldsymbol{Q}\tilde{\boldsymbol{d}} - \dot{\hat{\boldsymbol{d}}}^T\boldsymbol{\Gamma}^{-1}\tilde{\boldsymbol{d}}. \tag{16}$$

If the adaptive law is constructed as

$$\dot{\hat{\boldsymbol{d}}} = \boldsymbol{\Gamma}\boldsymbol{Q}\boldsymbol{R}^T\boldsymbol{s}, \tag{17}$$

one can achieve

$$\dot{V}_2 = -\boldsymbol{s}^T\left(\boldsymbol{K}_D + \boldsymbol{R}\boldsymbol{D}\boldsymbol{R}^T\right)\boldsymbol{s}. \tag{18}$$

By (18) and non-negativity of V_2, it can be obtained that all signals ($\boldsymbol{s}$, $\tilde{\boldsymbol{d}}$, $\boldsymbol{e}_p$, $\dot{\boldsymbol{e}}_p$, $\boldsymbol{F}_1$, and $\dot{\boldsymbol{s}}$) are bounded. By integrating both sides of (18) and the square integrability of $\boldsymbol{s}$ can be approved. Based on *Barbalat* lemma, $\boldsymbol{s}$ can be proven to converge to zero. It should be mentioned that $\tilde{\boldsymbol{d}}$ can only be guaranteed to be bounded.

C. Wind Speed Observer Design

In above subsection, the assumption $\boldsymbol{v}_w = 0$ is held, which is unsuitable as the quadrotor maneuver in a windy environment. In this subsection, a WSO is designed to compensate the wind disturbance. With respect to system (2), an intuitive WDO can be constructed as

$$\dot{\hat{\boldsymbol{v}}}_w = \boldsymbol{L}\left(\boldsymbol{a} - \frac{1}{m}\boldsymbol{F}_2 - g\boldsymbol{e}_3 + \frac{1}{m}\boldsymbol{\Lambda}\boldsymbol{v}\right) - \frac{1}{m}\boldsymbol{L}\boldsymbol{\Lambda}\hat{\boldsymbol{v}}_w, \tag{19}$$

where $\boldsymbol{\Lambda} = \boldsymbol{R}\boldsymbol{D}\boldsymbol{R}^T$ for simplicity, $\boldsymbol{L} \in \mathbb{R}^{3\times3}$ is a positive diagonal matrix, $\boldsymbol{F}_2$ is the modified control input provided in (21), and $\hat{\boldsymbol{v}}_w$ denotes the estimation of $\boldsymbol{v}_w$. By (19), $\dot{\tilde{\boldsymbol{v}}}_w = \frac{1}{m}\boldsymbol{L}\boldsymbol{\Lambda}\left(\boldsymbol{v}_w - \hat{\boldsymbol{v}}_w\right)$ can be achieved.

The acceleration measurement $\boldsymbol{a}$ is noisy, which may not be used in practice. In an attempt to circumvent this problem, an auxiliary state variable $\boldsymbol{\mu} \in \mathbb{R}^3$ is introduced as $\boldsymbol{\mu} = \hat{\boldsymbol{v}}_w - \boldsymbol{L}\boldsymbol{v}$.

The WSO is designed as

$$\begin{cases} \dot{\boldsymbol{\mu}} = -\frac{1}{m}\boldsymbol{L}\boldsymbol{\Lambda}\boldsymbol{\mu} - \frac{1}{m}\boldsymbol{L}\left(\boldsymbol{\Lambda}\boldsymbol{L}\boldsymbol{v} + \boldsymbol{F}_2 - \boldsymbol{\Lambda}\boldsymbol{v} + mg\boldsymbol{e}_3\right), \\ \hat{\boldsymbol{v}}_w = \boldsymbol{\mu} + \boldsymbol{L}\boldsymbol{v}, \\ \hat{\boldsymbol{F}}_{w2} = \boldsymbol{\Lambda}\hat{\boldsymbol{v}}_w, \end{cases} \tag{20}$$

where $\hat{\boldsymbol{F}}_{w2}$ denotes the estimation of $\boldsymbol{F}_{w2}$.

The translational controller is modified as

$$\boldsymbol{F}_2 = -mg\boldsymbol{e}_3 + m\boldsymbol{a}_r + \boldsymbol{K}_D\boldsymbol{s} + \boldsymbol{R}\boldsymbol{D}\boldsymbol{R}^T\boldsymbol{v}_r - \hat{\boldsymbol{F}}_{w2}. \tag{21}$$

Define estimation errors of the wind speed $\tilde{\boldsymbol{v}}_w = \boldsymbol{v}_w - \hat{\boldsymbol{v}}_w \in \mathbb{R}^3$ and the aerodynamic drag caused by wind $\tilde{\boldsymbol{F}}_{w2} = \boldsymbol{F}_{w2} - \hat{\boldsymbol{F}}_{w2}$. By combining (21) and (20), one can obtain

$$\dot{\tilde{\boldsymbol{v}}}_w = \dot{\boldsymbol{v}}_w - \frac{1}{m}\boldsymbol{L}\boldsymbol{\Lambda}\tilde{\boldsymbol{v}}_w. \tag{22}$$

Theorem 1. *Consider system (2) under controller (21) and WSO (20). If the WSO gain satisfies* $\lambda_m(\boldsymbol{L}) > \frac{1}{4}\left(\frac{\lambda_M(\boldsymbol{D})}{\lambda_m(\boldsymbol{D})}\right)^2$ *and the wind speed varies slowly relative to the system control frequency, the sliding variable* $\boldsymbol{s}$ *and the wind speed estimated error* $\tilde{\boldsymbol{v}}_w$ *will converge to zero exponentially as* $t \to \infty$.

Proof: By the assumption of slow variable wind speed ($\dot{\boldsymbol{v}}_w \approx 0$), from (22), one can obtain

$$\dot{\tilde{\boldsymbol{v}}}_w = -\frac{1}{m}\boldsymbol{L}\boldsymbol{\Lambda}\tilde{\boldsymbol{v}}_w. \tag{23}$$

Construct the followed Lyapunov function

$$V_3 = \frac{m}{2}\boldsymbol{s}^T\boldsymbol{s} + \frac{m}{2}\tilde{\boldsymbol{v}}_w^T\tilde{\boldsymbol{v}}_w. \tag{24}$$

By (21) and (23), the derivative of V_3 is obtained as

$$\dot{V}_3 = -\boldsymbol{s}^T\left(\boldsymbol{K}_D + \boldsymbol{\Lambda}\right)\boldsymbol{s} - \boldsymbol{s}^T\boldsymbol{\Lambda}\tilde{\boldsymbol{v}}_w - \tilde{\boldsymbol{v}}_w^T\boldsymbol{L}\boldsymbol{\Lambda}\tilde{\boldsymbol{v}}_w. \tag{25}$$

By using the conditions $\lambda(\boldsymbol{\Lambda}) = \lambda(\boldsymbol{D})$ and $-\boldsymbol{s}^T\boldsymbol{\Lambda}\tilde{\boldsymbol{v}}_w \le \lambda_m(\boldsymbol{D})\boldsymbol{s}^T\boldsymbol{s} + \frac{\lambda_M^2(\boldsymbol{D})}{4\lambda_m(\boldsymbol{D})}\tilde{\boldsymbol{v}}_w^T\tilde{\boldsymbol{v}}_w$, (25) can be written as

$$\begin{aligned} \dot{V}_3 \le & -\boldsymbol{s}^T\left(\boldsymbol{K}_D + \boldsymbol{\Lambda} - \lambda_m(\boldsymbol{D})\boldsymbol{I}\right)\boldsymbol{s} \\ & - \tilde{\boldsymbol{v}}_w^T\left(\boldsymbol{L}\boldsymbol{\Lambda} - \frac{\lambda_M^2(\boldsymbol{D})}{4\lambda_m(\boldsymbol{D})}\boldsymbol{I}\right)\tilde{\boldsymbol{v}}_w. \end{aligned} \tag{26}$$

By further using the conditions $-\boldsymbol{s}^T\boldsymbol{\Lambda}\boldsymbol{s} \le -\lambda_m(\boldsymbol{D})\boldsymbol{s}^T\boldsymbol{s}$ and $-\tilde{\boldsymbol{v}}_w^T\boldsymbol{L}\boldsymbol{\Lambda}\tilde{\boldsymbol{v}}_w \le -\lambda_m(\boldsymbol{L})\lambda_m(\boldsymbol{D})\tilde{\boldsymbol{v}}_w^T\tilde{\boldsymbol{v}}_w$, one can imply

$$\dot{V}_3 \le -\boldsymbol{s}^T\boldsymbol{K}_D\boldsymbol{s} - \left(\lambda_m(\boldsymbol{L})\lambda_m(\boldsymbol{D}) - \frac{\lambda_M^2(\boldsymbol{D})}{4\lambda_m(\boldsymbol{D})}\right)\tilde{\boldsymbol{v}}_w^T\tilde{\boldsymbol{v}}_w. \tag{27}$$

If the WSO gain satisfies $\lambda_m(\boldsymbol{L}) > \frac{1}{4}\left(\frac{\lambda_M(\boldsymbol{D})}{\lambda_m(\boldsymbol{D})}\right)^2$, it can be rendered that $\dot{V}_3 \le -\alpha V_3$, where $\alpha = \frac{2}{m}\min\left\{\lambda_m(\boldsymbol{K}_D), \lambda_m(\boldsymbol{L})\lambda_m(\boldsymbol{D}) - \frac{\lambda_M^2(\boldsymbol{D})}{4\lambda_m(\boldsymbol{D})}\right\}$. Obviously, the sliding variable $\boldsymbol{s}$ and wind speed estimated error $\tilde{\boldsymbol{v}}_w$ converge to zero exponentially.

Remark 2. *Traditional DO is usually designed to estimate the whole adverse effect caused by wind disturbance, i.e.* $\boldsymbol{R}\boldsymbol{D}\boldsymbol{R}^T\boldsymbol{v}_w$ *in this paper. The study presented in [22], [34] assumes that the norm of disturbance derivative is bounded by a constant, which determines the convergence range of system state. In this paper, the attitude information* $\boldsymbol{R}\boldsymbol{D}\boldsymbol{R}^T$ *is utilized in observer design, allowing to relax the assumption.*

It should be emphasized that if $\boldsymbol{R}\boldsymbol{D}\boldsymbol{R}^T\boldsymbol{v}_w$ is directly estimated [20], [22], [34], the assumption $\left\|\dot{\boldsymbol{F}}_{w2}\right\| \le \gamma$ (where γ is a positive constant) will lead to bounded convergence eventually ($\dot{V}_3 \le \delta_1 V_3 + \delta_2$, where δ_1 is a positive constant and δ_2 is proportional to γ^2 [16]). It is obvious that the bound of converged set relies on γ. It can be further proven that $\dot{\boldsymbol{F}}_{w2} = \dot{\boldsymbol{R}}\boldsymbol{D}\boldsymbol{R}^T\boldsymbol{v}_w + \boldsymbol{R}\boldsymbol{D}\dot{\boldsymbol{R}}^T\boldsymbol{v}_w + \boldsymbol{R}\boldsymbol{D}\boldsymbol{R}^T\dot{\boldsymbol{v}}_w$. As $\dot{\boldsymbol{v}}_w \approx 0$, $\left\|\dot{\boldsymbol{R}}\boldsymbol{D}\boldsymbol{R}^T\boldsymbol{v}_w + \boldsymbol{R}\boldsymbol{D}\dot{\boldsymbol{R}}^T\boldsymbol{v}_w\right\| \le \gamma$ is hold. The bound of converged set relies on the amplitude of external wind, attitude, and attitude velocity. In this work, by directly estimating $\boldsymbol{v}_w$, the final converged set can be compressed to zero ($\delta_2 = 0$). Thus, the WSO reduces the conservativeness of control.

V. Experimental Results

A. Experimental Setup

The translational and rotational controllers run onboard at 100 Hz and 1 kHz, respectively, with a STM32 processor. The position of the quadrotor UAV is provided by a motion capturing system running on a ground station, which is transmitted to the quadrotor through an ultra-wideband (UWB) transmission module at 50 Hz. The angular rate is measured by onboard IMU at 1 kHz. Three scenarios are arranged to evaluate the proposed drag-utilization scheme and WSO, respectively. The test trajectories in the first and second scenarios are set as circles that can be expressed as $\begin{bmatrix} r\sin(\frac{2\pi}{T}t) & r\cos(\frac{2\pi}{T}t) & h \end{bmatrix}^\top m$, where r, T, and h denote the radius, period, and flying height.

In the first scenario (Test #1 - Test #2), the performance of the drag-utilization scheme is verified using two different thrust-to-weight ratios (TWRs) quadrotors (Fig. 1) in high-speed flights. The radii of both tests are set as $1.8\ m$, and the trajectory velocities of the 6-inch quadrotor and 5-inch quadrotor are set as $4\ m/s$ (Test #1) and $5\ m/s$ (Test #2), respectively. The compared control systems consist of baseline controller (6), proposed drag-utilization scheme (11), adaptive estimation scheme (Section. IV-B.1, denoted as Adaptive$^+$), feedforward compensation scheme [4], [6] (denoted as Compensation), and DO-based control scheme [34].

In the second scenario (Test #3 - Test #4), the wind disturbance is injected and the designed WSO is activated. Two 380 W fans are placed at $[-2.5, 0.5, 1]\ m$ and $[-2.5, -0.5, 1]\ m$, along the direction of $\boldsymbol{e}_1$. Fig. 5 illustrates the wind field distribution, which is obtained by spatial

sampling through a digital anemometer AS8556. Notice that the sampling altitude is consistent with that of the quadrotor flight. The maximum wind speed is up to 6 m/s. The radii of the trajectories are set as 1 m (Test #3) and 1.8 m (Test #4), and the velocities are set as 2 m/s (Test #3) and 4 m/s (Test #4).

In the third scenario (Test #5), the estimation accuracy of the proposed WSO is analyzed, where the quadrotor is commanded to hover in the wind as depicted in Fig. 6(a). To improve the credibility [32], the ground-truth wind speed is obtained by taking the average of measurements over 10 independent time periods, and the estimated wind speed is obtained by taking the average of WSO measurements in 10 independent tests.

In each test, the irrelevant control parameters are set as the same for a fair comparison, which are summarized in Table I. $\boldsymbol{L}_{DO}$ denotes the observer gain designed in [34]. From Theorem 1, as long as $\boldsymbol{L}$ satisfies the theoretical condition, the system is stable. It should be emphasized that, although the convergence speed of WSO will increase with the increase of the observer gain, the noise problem will become more serious. The adjustment of the observer gain requires trade-off between the observer performance and stability in practice. The critical gain that is going to lead to "high-frequency vibration" phenomenon is taken as the optimal value. Since the design of WSO is derived from DO [34], their gains are set as the same for a fair comparison.

By fitting priori experimental data, the drag coefficients $\boldsymbol{D}$ are obtained as $diag\left[0.32, 0.31, 0\right]$ and $diag\left[0.28, 0.26, 0\right]$ for 6-inch and 5-inch quadrotors, respectively. Similar to the work presented in [6], the drag along $\boldsymbol{e}_3$ is ignored due to its minor influence. Moreover, in order to increase the conviction, each test (Test #1 – Test #4) is repeated three times and the quantitative compared results (Section. V-C) are calculated. The test represented by the median is selected.

TABLE I
CONTROLLER PARAMETERS

	Parameters
5-inch	$\boldsymbol{K}_P = diag\left[2.7, 2.6, 1.6\right], \boldsymbol{K}_D = diag\left[10.8, 10.4, 6.4\right]$
	$\boldsymbol{K}_R = diag\left[10, 10, 4\right], \boldsymbol{K}_\omega = diag\left[40, 40, 16\right]$
	$\boldsymbol{\Gamma} = diag\left[0.07, 0.07, 0.07\right], \boldsymbol{L}_{DO} = diag\left[0.4, 0.4, 0.4\right]$
	$\boldsymbol{L} = diag\left[0.4, 0.4, 0.4\right]$
6-inch	$\boldsymbol{K}_P = diag\left[2, 2, 1.6\right], \boldsymbol{K}_D = diag\left[8, 8, 6.4\right]$
	$\boldsymbol{K}_R = diag\left[10, 10, 4\right], \boldsymbol{K}_\omega = diag\left[40, 40, 16\right]$
	$\boldsymbol{\Gamma} = diag\left[0.05, 0.05, 0.05\right], \boldsymbol{L}_{DO} = diag\left[0.3, 0.3, 0.3\right]$

B. Experimental Results

1) Scenario #1: In absence of wind disturbance, the tracking performance with respect to 6-inch and 5-inch quadrotors during high-speed flights is presented in Fig. 4. Due to the large flying radius, the improved accuracy is not visually obvious. The results of quantification will be presented in the next subsection. Furthermore, the final converged

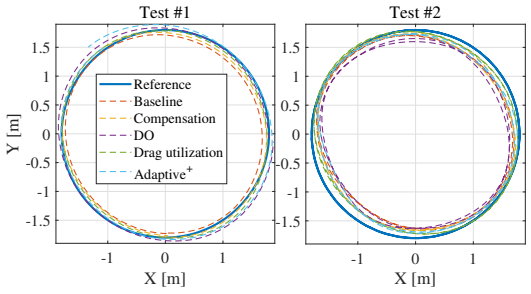

Fig. 4. The tracking performance of 6-inch quadrotor with 4 m/s and 13.23 m/s^2 and 5-inch quadrotor with 5 m/s and 17.00 m/s^2.

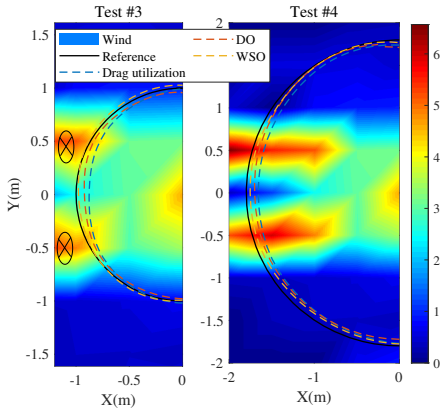

Fig. 5. 5-inch quadrotor maneuvers in a wind field with $\boldsymbol{v} = 2$ m/s, $r = 1$ m (Test #3) and $\boldsymbol{v} = 4$ m/s, $r = 1.8$ m (Test #4).

valus of $\hat{\boldsymbol{d}}$ in Adaptive$^+$ method are $diag\left[0.43, 0.42, 0\right]$ and $diag\left[0.55, 0.39, 0\right]$ for 6-inch and 5-inch quadrotors.

2) Scenario #2: Fig. 5 shows the compared results as the wind disturbance is involved. The actual trajectories are deviated to the East with previous drag-utilization and DO, while the flight trajectories and the preset circle path overlap more precisely as WSO works.

3) Scenario #3: The WSO estimated wind speed and the position tracking error $\boldsymbol{e}_{px}$ along the wind direction are shown in Fig. 6(b). The standard deviation (STD) of the 10 estimated wind speeds remains below 0.3 and $\boldsymbol{e}_{px}$ stays close to zero over the entire period. However, the estimation error looks not satisfying.

C. Experimental Analysis

To evaluate the tracking performance quantitatively, Root mean square error (RMSE) [1] μ is defined as

$$\mu = \sqrt{\frac{1}{n}\sum_{i=1}^{n}\left\|\boldsymbol{p}_i - \boldsymbol{p}_{d,i}\right\|^2}, \tag{28}$$

where n is the size of data set collected during flights.

Table II summarizes quantified compared results. More visually, Fig. 7 presents the performance improvement (RMSE) of the proposed method relative to other compared methods. The performance improvement is calculated by $\frac{\mu_{pro}-\mu_{com}}{\mu_{com}} \times$

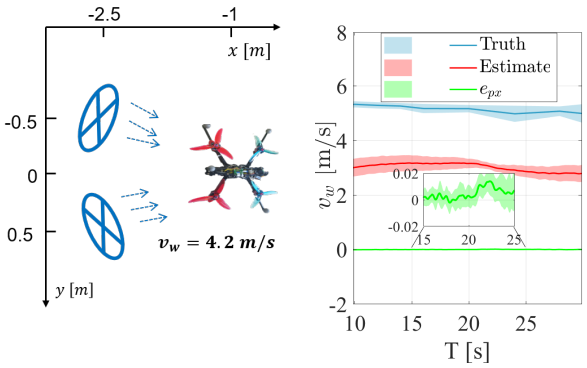

(a) Conceptual graphs.

(b) The estimated wind speed of WSO. The colored shaded area represents the STD of 10 independent tests.

Fig. 6. 5-inch quadrotor hovering in the wind.

TABLE II

ROOT MEAN SQUARE ERROR μ. (UNIT:m)

		RMSE
Test #1: 6-inch *with* $\boldsymbol{v} = 4\ m/s$	Baseline	0.0972
	Compensation	0.0758
	DO	0.0972
	Drag-utilization	**0.0652**
	Adaptive$^+$	0.1172
Test #2: 5-inch *with* $\boldsymbol{v} = 5\ m/s$	Baseline	0.1590
	Compensation	0.1348
	DO	0.1941
	Drag-utilization	**0.0887**
	Adaptive$^+$	0.1201
Test #3: 5-inch *with 2 m/s, in wind*	Drag-utilization	0.0936
	DO	0.0579
	WSO	**0.0529**
Test #4: 5-inch *with 4 m/s, in wind*	Drag-utilization	0.1306
	DO	0.1124
	WSO	**0.0918**

100%, where μ_{pro} denotes the RMSE of the proposed method and μ_{com} denotes the RMSE of the compared one.

1) Scenario #1: It is highlighted that the drag-utilization method achieves $16.9\% - 44.3\%$ (RMSE) improvements for 6-inch quadrotor, and $26.1\% - 54.3\%$ (RMSE) enhancements for 5-inch quadrotor.

In contrast to the feedforward compensation scheme [4], [6], the RMSEs are reduced by 16.9% (6-inch) and 34.2% (5-inch) under drag-utilization scheme, since the drag-utilization scheme is capable of increasing the control gains, leading to better tracking performance. In [34], the assumption of slow variable disturbance is held. However, the aerodynamic drag at high speed varies with the states (speed and attitude) of the quadrotor, which does not satisfy the assumption of slow change in [34]. Thus, it is reasonable that the tracking accuracy is not improved when DO [34] works. With the help of adaptive estimation, although the coefficients do not need to be identified, the tracking performance of quadrotor is not satisfying, even worse than baseline controller for 6-inch quadrotor. In simulation, usually very high $\boldsymbol{\Gamma}$ can guarantee the performance of adaptive control. Whereas, due to the noise in tracking error $\boldsymbol{s}$, delays, finite control frequency, and actuator limitation in reality, the adaptive gain can only be set as a relatively small value, inducing poor performance.

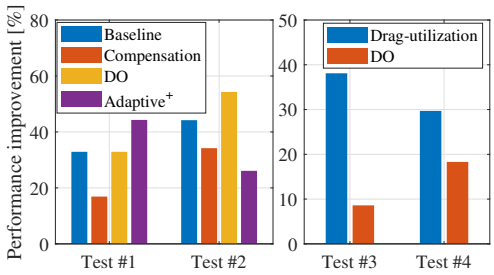

Fig. 7. Performance improvement (RMSE) of the proposed method relative to compared methods.

2) Scenario #2: As the wind disturbance is involved, compared with the scheme without any anti-disturbance measures, the proposed WSO achieves 38.1% (RMSE) improvements for 2 m/s, and 29.7% (RMSE) enhancements for 4 m/s, which demonstrate the anti-disturbance peroformance of the proposed WSO. When comparing to DO enhanced method, the proposed WSO only achieves 8.6% (RMSE) improvements for 2 m/s. The phenomenon is consistent with the statement in Remark 2. By directly estimating $\boldsymbol{v}_w$, the attitude information ($\boldsymbol{RDR}^T$) can be fully utilized. When the quadrotor flies at a small attitude (2 m/s, nearly 0.39 rad), and $\boldsymbol{RDR}^T$ is close to $\boldsymbol{D}$, which means the WSO will degrade into traditional DO. As flying at 4 m/s (nearly 0.74 rad), the improvement can achieve 18.3% (RMSE) which further reveals the advantage of WSO will become more obvious in a larger attitude.

3) Scenario #3: Although the wind speed estimated error is roughly 40%, the position tracking error can remain very small. Two factors induce the estimated error. On the one hand, the fitted drag coefficient $\boldsymbol{D}$ has deviations. On the other hand, due to the existence of other uncertainties besides wind, the performance of the WSO can be affected. The estimation of WSO captures not only the wind disturbance, but also the effects of uncertainties.

VI. LIMITATIONS

The estimated accuracy of wind speed is greatly affected by inaccurate $\boldsymbol{D}$ and other uncertainties. It is noticed that different experimental trajectories cause different drag $\boldsymbol{D}$ [6]. How to obtain high-precision $\boldsymbol{D}$ (preferably in an online paradigm to avoid advance parameter identification) is an interesting research topic. Moreover, extract the wind disturbance from multiple disturbances will be helpful to improve the estimation accuracy of WSO, so that the estimated wind speed can be used for other purpose (e.g. exploring the wind distribution at high altitude). Lastly, the motor delay or amplitude limit, which may lead to imperfect thrust realization is not considered. Future work will pursue to address these challenges.

VII. Conclusion

In this work, a drag-utilization scheme is presented to improve the tracking performance of the quadrotors in high-speed flights. In comparison of the standard feedforward compensation scheme, the drag-utilization scheme can improve the convergence speed of tracking errors with less noise. The wind disturbance is further considered. A WSO is designed and integrated in the baseline controller to reject wind disturbance. Different from previous works, the WSO reduces the conservativeness of control. In experiments, to fully demonstrate the performance of the proposed drag-utilization scheme and WSO, two quadrotors with different TWRs are used. Results show that the proposed control scheme is superior than other state-of-art algorithms.

References

[1] A. Loquercio, E. Kaufmann, R. Ranftl, M. Müller, V. Koltun, and D. Scaramuzza, "Learning high-speed flight in the wild," *Science Robotics*, vol. 6, no. 59, p. eabg5810, 2021.

[2] X. Yu, Y. Zhu, J. Qiao, and L. Guo, "Anti-disturbance controllability analysis and enhanced anti-disturbance controller design with application to flexible spacecraft," *IEEE Transactions on Aerospace and Electronics Systems*, vol. 57, no. 5, pp. 3393–3404, 2021.

[3] M. Elfeky, M. Elshafei, A.-W. A. Saif, and M. F. Al-Malki, "Modeling and simulation of quadrotor UAV with tilting rotors," *International Journal of Control, Automation and Systems*, vol. 14, no. 4, pp. 1047–1055, 2016.

[4] P. Foehn, D. Brescianini, E. Kaufmann, T. Cieslewski, M. Gehrig, M. Muglikar, and D. Scaramuzza, "AlphaPilot: Autonomous Drone Racing," in *Proceedings of Robotics: Science and Systems*, Corvalis, USA, 2020.

[5] D. Mellinger and V. Kumar, "Minimum snap trajectory generation and control for quadrotors," in *Proceedings of 2011 IEEE International Conference on Robotics and Automation (ICRA), Shanghai, China*, 2011, pp. 2520–2525.

[6] M. Faessler, A. Franchi, and D. Scaramuzza, "Differential flatness of quadrotor dynamics subject to rotor drag for accurate tracking of high-speed trajectories," *IEEE Robotics and Automation Letters*, vol. 3, no. 2, pp. 620–626, 2017.

[7] G. Torrente, E. Kaufmann, P. Föhn, and D. Scaramuzza, "Data-driven MPC for quadrotors," *IEEE Robotics and Automation Letters*, vol. 6, no. 2, pp. 3769–3776, 2021.

[8] S. Sun, A. Romero, P. Foehn, E. Kaufmann, and D. Scaramuzza, "A comparative study of nonlinear MPC and differential-flatness-based control for quadrotor agile flight," *arXiv preprint arXiv:2109.01365*, 2021.

[9] M. Bisheban and T. Lee, "Geometric adaptive control with neural networks for a quadrotor in wind fields," *IEEE Transactions on Control Systems Technology*, vol. 29, no. 4, pp. 1533–1548, 2021.

[10] X. Yu, L. Guo, Y. Zhang, and J. Jiang, *Autonomous Safety Control of Flight Vehicles*. CRC Press, Taylor & Francis Group, 2021.

[11] A.-W. A. Saif, "Feedback linearisation control of quadrotor with tiltable rotors under wind gusts," *International Journal of Advanced and Applied Sciences*, vol. 4, no. 10, pp. 150–159, 2017.

[12] A. Tagliabue, A. Paris, S. Kim, R. Kubicek, S. Bergbreiter, and J. P. How, "Touch the wind: Simultaneous airflow, drag and interaction sensing on a multirotor," in *Proceedings of 2020 IEEE/RSJ International Conference on Intelligent Robots and Systems (IROS), Las Vegas, USA*, 2020, pp. 1645–1652.

[13] M. Schulz, F. Augugliaro, R. Ritz, and R. D'Andrea, "High-speed, steady flight with a quadrocopter in a confined environment using a tether," in *Proceedings of 2015 IEEE/RSJ International Conference on Intelligent Robots and Systems (IROS), Hamburg, Germany*, 2015, pp. 1279–1284.

[14] J.-M. Kai, G. Allibert, M.-D. Hua, and T. Hamel, "Nonlinear feedback control of quadrotors exploiting first-order drag effects," *IFAC-PapersOnLine*, vol. 50, no. 1, pp. 8189–8195, 2017.

[15] P. Martin and E. Salaün, "The true role of accelerometer feedback in quadrotor control," in *Proceedings of 2010 IEEE international Conference on Robotics and Automation (ICRA), Anchorage, USA*, 2010, pp. 1623–1629.

[16] J. Jia, K. Guo, X. Yu, L. Guo, and L. Xie, "Agile flight control under multiple disturbances for quadrotor: Algorithms and evaluation," *IEEE Transactions on Aerospace and Electronic Systems*, In Press, DOI: 10.1109/TAES.2022.3143781, 2022.

[17] C. D. Johnson, "Disturbance-accommodating control: An overview," in *Proceedings of 1986 American Control Conference, Seattle, USA*, 1986, pp. 526–536.

[18] J.-J. E. Slotine, W. Li *et al.*, *Applied Nonlinear Control*. Prentice hall Englewood Cliffs, NJ, 1991, vol. 199, no. 1.

[19] T. Tomić, P. Lutz, K. Schmid, A. Mathers, and S. Haddadin, "Simultaneous contact and aerodynamic force estimation (s-cafe) for aerial robots," *The International Journal of Robotics Research*, vol. 39, no. 6, pp. 688–728, 2020.

[20] X. Lyu, J. Zhou, H. Gu, Z. Li, S. Shen, and F. Zhang, "Disturbance observer based hovering control of quadrotor tail-sitter VTOL UAVs using H_∞ synthesis," *IEEE Robotics and Automation Letters*, vol. 3, no. 4, pp. 2910–2917, 2018.

[21] A. Castillo, R. Sanz, P. Garcia, W. Qiu, H. Wang, and C. Xu, "Disturbance observer-based quadrotor attitude tracking control for aggressive maneuvers," *Control Engineering Practice*, vol. 82, pp. 14–23, 2019.

[22] K. Guo, J. Jia, X. Yu, L. Guo, and L. Xie, "Multiple observers based anti-disturbance control for a quadrotor UAV against payload and wind disturbances," *Control Engineering Practice*, vol. 102, p. 104560, 2020.

[23] S. Zhou, K. Guo, X. Yu, L. Guo, and L. Xie, "Fixed-time observer based safety control for a quadrotor UAV," *IEEE Transactions on Aerospace and Electronics Systems*, vol. 57, no. 5, pp. 2815–2825, 2021.

[24] B. Morrell, M. Rigter, G. Merewether, R. Reid, R. Thakker, T. Tzanetos, V. Rajur, and G. Chamitoff, "Differential flatness transformations for aggressive quadrotor flight," in *Proceedings of 2018 IEEE International Conference on Robotics and Automation (ICRA), Brisbane, Australia*, 2018, pp. 5204–5210.

[25] M. Watterson and V. Kumar, "Control of quadrotors using the hopf fibration on SO(3)," in *Robotics Research*, 2020, pp. 199–215.

[26] E. Tal and S. Karaman, "Accurate tracking of aggressive quadrotor trajectories using incremental nonlinear dynamic inversion and differential flatness," *IEEE Transactions on Control Systems Technology*, vol. 29, no. 3, pp. 1203–1218, 2020.

[27] S. Zhou, M. K. Helwa, and A. P. Schoellig, "Deep neural networks as add-on modules for enhancing robot performance in impromptu trajectory tracking," *The International Journal of Robotics Research*, vol. 39, no. 12, pp. 1397–1418, 2020.

[28] A.-W. A. Saif, A. Aliyu, M. A. Dhaifallah, and M. Elshafei, "Decentralized backstepping control of a quadrotor with tilted-rotor under wind gusts," *International Journal of Control, Automation and Systems*, vol. 16, no. 5, pp. 2458–2472, 2018.

[29] P. Foehn, A. Romero, and D. Scaramuzza, "Time-optimal planning for quadrotor waypoint flight," *Science Robotics*, vol. 6, no. 56, p. eabh1221, 2021.

[30] L. Guo and W. H. Chen, "Disturbance attenuation and rejection for systems with nonlinearity via DOBC approach," *International Journal of Robust and Nonlinear Control*, vol. 15, no. 3, pp. 109–125, 2005.

[31] D. Hentzen, T. Stastny, R. Siegwart, and R. Brockers, "Disturbance estimation and rejection for high-precision multirotor position control," in *Proceedings of 2019 IEEE/RSJ International Conference on Intelligent Robots and Systems (IROS), Macau, China*, 2019, pp. 2797–2804.

[32] M. Bangura, X. Hou, G. Allibert, R. Mahony, and N. Michael, "Supervisory control of multirotor vehicles in challenging conditions using inertial measurements," *IEEE Transactions on Robotics*, vol. 34, no. 6, pp. 1490–1501, 2018.

[33] T. Lee, M. Leok, and N. H. Mcclamroch, "Control of complex maneuvers for a quadrotor UAV using geometric methods on $\mathrm{SE}(3)$," *Mathematics*, vol. 15, no. 2, pp. 391–408, 2010.

[34] K. Guo, J. Jia, X. Yu, and L. Guo, "Dual-disturbance observers-based control of UAV subject to internal and external disturbances," in *Proceedings of 2019 Chinese Automation Congress (CAC), Hangzhou, China*, 2019, pp. 2683–2688.